USCAP

Check for updates

ARTICLE

YY1 alleviates lupus nephritis-induced renal injury by reducing the Th17/Treg cell ratio via the IFN-γ/Fra2 axis

Bi Wang[1,4], Xinhui Jiang[2,4], Yuhong Li[2], Haixia Xu[2], Bei Ying[2], Jie Qiu[2], Zhi Huang[3✉] and Xiaoshan Shao [2✉]

Lupus nephritis (LN) is associated with extensive injury and nephron loss in the afflicted kidney. Evidence has revealed the involvement of dysregulated Yin Yang 1 (YY1), a reported inflammatory modulator, in LN-induced kidney injury, and our microarray profile identified downregulated YY1 expression. Therefore, this study explored the functional relevance and mechanism of YY1 in LN-induced kidney injury. LN was modeled in mice by intraperitoneal injection of pristane, and Jurkat cells (CD41 human T lymphocytes) were activated with TNF-α to mimic the inflammatory environment found in LN. The expression patterns of YY1 and bioinformatics predictions of the downstream factor IFN-γ were confirmed in renal tissues from the mice with LN using qRT-PCR and Western blot analyses. The contents of proinflammatory cytokines in mouse serum samples and cell supernatants were determined using enzyme-linked immunosorbent assays (ELISAs). Ectopic expression and depletion approaches were subsequently used in vitro and in vivo to examine the effects of the YY1/IFN-γ/Fra2/PARP-1/FOXO1 axis on TNF-α-induced inflammation and LN-induced kidney injury. The results showed downregulated expression of YY1 and FOXO1 in the kidney tissues of the mice with LN. Increased proinflammatory factor production was observed in the mice with LN and TNF-α-treated Jurkat cell supernatant, accompanied by increased cell apoptosis and a high ratio of Th17/Treg cells, and these effects were reversed by YY1 restoration. YY1 was further shown to inhibit IFN-γ expression and thereby downregulate Fra2 expression. Fra2 depletion then inhibited PARP-1 expression and promoted FOXO1 expression to suppress cell apoptosis and the release of inflammatory factors. Collectively, our findings revealed that YY1 may alleviate LN-induced renal injury via the IFN-γ/Fra2/PARP-1/FOXO1 axis.

INTRODUCTION

Lupus nephritis (LN), a critical cause of acute/chronic kidney injury that leads to end-stage renal disease, is characterized by aberrantly activated innate and adaptive immune responses, dysregulated inflammatory signaling pathways, and increased cytokine production[1]. Approximately 60% of patients with systemic lupus erythematosus (SLE) suffer from LN, and current therapeutic modalities include high-dose corticosteroids and cytotoxic medications; however, these treatments result in severe side effects, and remission rates remain high[2]. Despite the emergence of therapeutic strategies for LN, the renal outcomes remain unsatisfactory, and various promising therapies have failed in clinical trials, indicating the need for improved treatments[3]. Since patients with LN are usually unresponsive to the initial treatment, individualized management of patients with LN and appropriate treatments are urgently needed[4].

Yin Yang 1 (YY1) is a ubiquitously expressed zinc-finger DNA/RNA-binding transcription factor that mediates the expression of various cellular genes through interactions with different regulatory proteins, including transcription factors, coactivators and corepressors[5]. Importantly, YY1, which is involved in modulating cell apoptosis, cell cycle distribution, inflammatory responses, and cellular metabolism, consists of an N-terminal

intrinsically disordered fragment and a C-terminal domain responsible for DNA binding[6,7]. Moreover, YY1 expression was shown to be upregulated in mesangial cells of early diabetic renal lesions and downregulated in later stages, while glomerulosclerosis was attenuated by overexpression of YY1 and aggravated by YY1 knockdown[8]. According to results from the TRRUST database reported prior to our investigation, interferon γ (IFN-γ) transcription was predicted to be suppressed by YY1. IFN-γ has been proposed as an effective biomarker of disease activity, renal injury, and the activity of pathological lesions in patients with SLE[9]. In addition, the expression of Fos-related antigen-2 (Fra2), a promising drug target for treatment of LN-induced podocyte injury, is upregulated by IFN-γ[10].

Furthermore, downregulated Fra-2 expression was shown to alleviate retinal damage induced by light by inhibiting poly (ADP-ribose) polymerase 1 (PARP-1), a corepressor of Forkhead box O1 (FOXO1)[11,12]. FOXO1, a member of the FOXO subfamily of Forkhead transcription factors, is evolutionarily conserved and is involved in various biological activities, including cell cycle arrest, cell apoptosis and cellular metabolism[13–15]. Intriguingly, evidence has increasingly revealed the involvement of FOXO1 and associated pathways in diabetic kidney disease[16–18], but the potential role of FOXO1 in LN-induced renal injury remains

---

[1]School of Basic Medical Science, Guizhou Medical University, Guiyang 550002, P.R. China. [2]Department of Nephrology and Immunology, Guiyang Maternal & Child Health Care Hospital, Guiyang 550003, P. R. China. [3]Department of Interventional Radiology, The Affiliated Hospital of Guizhou Medical University, Guiyang 550002, P.R. China. [4]These authors contributed equally: Bi Wang, Xinhui Jiang. ✉email: doctor@huangzhi.com; sxs22@qq.com

unclear. Hence, we hypothesized that YY1 might alleviate LN-induced renal injury by modulating the possible downstream IFN-γ/Fra2/PARP-1/FOXO1 pathway.

MATERIALS AND METHODS
Ethics approval
Informed consent was provided by the enrolled subjects under a protocol approved by the Ethics Committee of Guiyang Maternal & Child Health Care Hospital. The experimental procedures involving animals were approved by the Animal Ethics Committee of Guiyang Maternal & Child Health Care Hospital. All animals received humane care according to the Guide for the Care and Use of Laboratory Animals published by the US National Institute of Health.

Network pharmacology analysis
The LN-related microarray dataset GSE82221 was retrieved from the Gene Expression Omnibus (GEO) database and included 25 samples from controls and 15 samples from patients with LN. Differentially expressed genes in samples from the patients with LN were selected with |logFoldChange| > 0.2 and $p < 0.05$ using the "limma" package in R language. YY1 expression in the control samples and the samples from the patients with LN was verified using the "boxplot" package in R language. Downstream regulatory genes of YY1 were predicted using the TRRUST database.

Clinical samples
Thirty Chinese patients with LN were enrolled at Guiyang Maternal & Child Health Care Hospital. Patients were diagnosed with LN based on the presence of persistent proteinuria (0.5 g/24 h), cell casting, persistent hematuria, or biopsy evidence. Patients were excluded if they were diagnosed with chronic renal failure, uncontrolled hypertension, chronic infection, malignant tumor, or diabetes mellitus. No patient had undergone corticosteroid or immunosuppressant therapies at least 3 months before sample collection. Another 30 healthy volunteers were included as controls.

Blood samples (5 mL) were collected from each patient in the fasting state and placed in a tube containing 0.2 mL of heparin sodium. Serum was stored at −70 °C. Peripheral blood mononuclear cells were obtained through Ficoll density gradient centrifugation. The cells were suspended in RPMI 1640 medium (2×10^6 cells/mL) with 100 U/mL penicillin, 100 μg/mL streptomycin, 2 mM glutamine and 10% heat-inactivated fetal bovine serum (FBS) (Gibco BRL, Gaithersburg, MD), and the suspension was transferred to 24-well plates. The cells were cultured with 50 ng/mL phorbol myristate acetate and 1 μg/mL ionomycin in the presence of monensin (1.7 μg/mL, Sigma, St. Louis, MO) for 4 h at 37 °C with 5% CO_2.

Cell treatment
Jurkat cells (a CD41 human T lymphocyte cell line) were cultured in RPMI 1640 medium with 10% FBS, 2 mM glutamine and 100 U penicillin–streptomycin. Upon reaching 65% confluence, the cells were passaged. Cells at passage 2 or 3 were used for interference experiments. Jurkat cells were exposed to 100 pM recombinant human tumor necrosis factor-α (TNF-α; Peprotech, Rocky Hill, NJ) to activate inflammation-related pathways and trigger apoptosis, thus simulating the microenvironment of LN (hereafter referred to as LN cells). The recombinant human Fra2 protein was purchased from Abcam (Cambridge, UK).

Based on the manufacturer's manual, lentivirus was constructed using the lentivirus vector system pHBLV-U6-Puro (Hanbio Co., Ltd., Shanghai, China). Short hairpin RNAs (shRNAs) against YY1[19], IFN-γ, Fra2, PARP-1[20] and FOXO1[21] and corresponding lentiviruses were designed and constructed. Negative control (NC) lentivirus carrying a scramble shRNA (Scr shRNA) was also designed. LN cells were then grouped and infected with lentivirus shuttling gene overexpression plasmids or shRNA-carrying plasmids to overexpress or knock down the expression of the tested genes.

Specifically, the expression vectors were transfected into 293 T cells utilizing Lipofectamine 3000 reagent (Invitrogen, Carlsbad, CA), and the cell culture supernatant was centrifuged 48 h later to collect the corresponding lentivirus. For lentivirus-mediated transduction, Jurkat cells were seeded in 6-well plates (2 mL/well) and, upon reaching 50% confluence, transduced with lentivirus at a titer greater than 10^7 TU/mL. After 48 h of incubation, stably transduced cells were screened using G418

for 2 weeks, followed by reverse transcription quantitative polymerase chain reaction (qRT-PCR) and Western blot analyses.

qRT-PCR
Total RNA was extracted with TRIzol (15596–018, Beijing Solarbio Technology, Beijing, China) according to the manual, followed by the determination of the RNA concentration. Complementary DNA (cDNA) was synthesized using an RNA reverse transcription kit (KR116, Tiangen Biotechnology, Beijing, China). An Applied Biosystems ViiA™ 7 fluorescence qPCR instrument (Life Technologies, Inc., Applied Biosystems, Foster City, CA) and miRNA fluorescence qPCR (AQ101–02, Full Gold, Beijing, China) were employed. Relative transcription levels of target genes were calculated using the $2^{-\Delta\Delta CT}$ method, with β-actin serving as an internal reference. Primer sequences are shown in Supplementary Table 1.

Western blot analysis
Total proteins were extracted from cells or tissues using efficient radioimmunoprecipitation assay lysis buffer (R0010, Solarbio) with protease inhibitor and lysed at 4 °C for 15 min. The protein concentration was measured using a bicinchoninic acid kit (20201ES76, Yeasen Biotech, Shanghai, China) and adjusted to 1 μg/μL. Proteins were directly loaded onto 10–12% sodium dodecyl sulfate–polyacrylamide gel electrophoresis gels and transferred onto polyvinylidene fluoride membranes (0.2 μm, Bio-Rad Laboratories, Inc., Hercules, MA). The membranes were blocked with 5% skim milk powder (w/v) in 1% Tris-buffered saline containing Tween-20 (TBST) at room temperature for 1 h and incubated with primary antibodies (listed in Supplementary Table 2) at 4 °C overnight. The membranes were incubated with horseradish peroxidase (HRP)-conjugated goat anti-rabbit immunoglobulin G (IgG) secondary antibody (ab205718, 1:20000, Abcam) or goat anti-mouse secondary antibody (ab6789, 1:5000, Abcam) at room temperature for 1 h. Immunoblots were observed using Immobilon Western Chemiluminescence HRP substrate (Millipore Corporation, Billerica, MA) and a Bio-Rad Chemi Doc MP instrument. GAPDH was used as the internal reference. The optical density was analyzed using ImageJ 6.0 software (National Institutes of Health, Bethesda, MD).

Flow cytometry
T helper 17 (Th17) and T regulatory (Treg) cell differentiation was detected. Lymphocytes were incubated with 3 μL of phorbol-12-myristate-13-acetate (PMA) and elaiomycin (Dakewe Biotech, Shenzhen, China), rinsed with BD Pharmingen™ staining buffer solution (BD, NJ), and fixed with BD Pharmingen™ Mouse Foxp3 fixative buffer solution. After centrifugation at $250 \times g$ and rinsing with preheated BD Pharmingen™ Mouse Foxp3 permeabilization buffer, lymphocytes interacted with 20 μL of Th17/Treg cell mixture. Cells were suspended in 1 mL of BD Pharmingen™ staining buffer solution and analyzed using a FACSCanto II flow cytometer (BD Biosciences, San Jose, CA). Lymphocytes, CD4 cells, CD4/IL-17 cells (Th17) and CD4/Foxp3 cells (Treg) were identified using forward scattering and lateral scattering.

For analysis of cell apoptosis, cells were trypsinized and centrifuged (1000 r/min) for 5 min. The sample was then fixed with 70% ethanol precooled at 4 °C. Cells (1×10^6 cells/mL) were stained with 10 mL of Annexin V-fluorescein isothiocyanate/propidium iodide (FITC/PI) (556547, Shanghai Shuojia Biotechnology, Shanghai, China) for 15–30 min at 4 °C. FITC and PI were detected using a flow cytometer (Type XL, Coulter) at wavelengths of 530 nm and >575 nm with an excitation wavelength of 480 nm.

Dual-luciferase reporter gene assay
The wild-type (WT) YY1 binding site in the 3′ untranslated region of the IFN-γ promoter was inserted into a dual-luciferase reporter gene plasmid, and the corresponding mutant (MUT) plasmid containing MUT binding sites for YY1 was constructed; the plasmids are referred to as PmirGLO-IFN-γ-WT and PmirGLO-IFN-γ-MUT. The reporter plasmid oe-YY1 and NC plasmid were cotransfected into lymphocytes for 24 h. Following lysis, the supernatant was collected through centrifugation at 12,000 rpm for 1 min. Luciferase activity was measured using a Dual-Luciferase Reporter Assay System (E1910, Promega, Madison, WI), with 100 μL of both firefly and Renilla luciferase working solutions added to each sample. Relative luciferase activity = firefly luciferase activity / Renilla luciferase activity.

Chromatin immunoprecipitation (ChIP) assay

ChIP assays were performed using an EZ-Magna ChIP TMA kit (Millipore). Upon reaching 70–80% confluence, cells were treated with 1% formaldehyde for 10 min to generate DNA-protein crosslinking, followed by the addition of glycine. The supernatant was removed through centrifugation at 2000 rpm for 5 min. The cells were collected and lysed at 4 °C using SDS lysis buffer. After the addition of the protease inhibitor complex, 500–1000 bp fragments were obtained through ultrasonication. An NC antibody against IgG (ab133470, 1:1000, Abcam) and a target protein-specific antibody against YY1 (1:1000, sc-7341, Santa Cruz, CA) were added and incubated overnight at 4 °C. The DNA-protein complex was precipitated using Protein A Agarose/Sepharose. The nonspecific proteins were removed from the complex by rinsing, and the crosslinks in the complex were reversed at 65 °C overnight. DNA fragments were extracted, purified, and retrieved using phenol/chloroform. The binding between YY1 and the IFN-γ promoter region was detected by qRT–PCR using specific primers for the IFN-γ promoter region.

Coimmunoprecipitation (Co-IP) assay

Co-IP was performed to detect the interaction between endogenous PARP-1 and FOXO1. Lymphocytes were lysed using Pierce IP buffer solution (1% Triton X-100, 150 mM NaCl, 1 mM ethylenediaminetetraacetic acid, and 25 mM Tris HCl pH 7.5) with protease and phosphatase inhibitors. Cell lysates were incubated with antibodies against PARP-1 (#9532 S, 1:100, Cell Signaling Technology, Danvers, MA) and mouse anti-IgG (3420, 1:50, Cell Signaling Technology) at 4 °C overnight. After the addition of Protein G beads (Dynabeads, Thermo Fisher, Waltham, MA), the sample was rotated slowly for 8 h at 4 °C, followed by Western blot analysis.

Glutathione S-transferase (GST) pulldown assay

The GST fusion protein was expressed in the *Escherichia coli* BL-21 bacterial strain using the pGEX vector system. The extract of infected Jurkat cells was incubated with various GST fusion proteins fixed on glutathione-agarose in lysis buffer A at 4 °C for 4 h to detect binding in vitro. The beads were washed 4 times using the same buffer solution, followed by Western blot analysis.

Establishment of mouse models of LN

The purchased 8-week-old female specific pathogen-free (SPF) BALB/c mice (weight: 21 ± 3 g) were provided with sterile food and water and housed with an artificial 12 h light-dark cycle in an SPF environment. A maximum of five mice were placed in each cage.

Female BALB/c mice were intravenously injected with 0.5 mL of pristane (molecular formula: $C_{19}H_{40}$, molecular weight: 268.52, density: 0.783) alone or in combination with an intravenous injection of oe-YY1/oe-NC lentivirus three months later, referred to as the LN, oe-YY1 and oe-NC groups ($n = 8$), to investigate the effect of YY1 on LN-induced renal injury. Mice intraperitoneally injected with normal saline were used as the control group ($n = 8$).

For determination of whether YY1 affected LN-induced renal injury by mediating Th17 and Treg cell differentiation *via* FOXO1, female BALB/c mice were intravenously injected with 0.5 mL of pristine with/without further intravenous injection with lentivirus three months later to manipulate the expression of FOXO1 and YY1 alone or in combination (sh-FOXO1 + oe-NC, oe-YY1 + sh-NC, oe-YY1 + sh-FOXO1 and oe-NC + sh-NC). In addition, mice intraperitoneally injected with normal saline were used as the control group. Eight mice were included in each group.

Enzyme-linked immunosorbent assay (ELISA)

The contents of TNF-α, interleukin-6 (IL-6) and IL-1β in mouse serum and cell supernatants were measured according to the manuals of the TNF-α, IL-6 and IL-1β kits (MTA00B, D6050, MLB00C, R&D Systems, Minneapolis, MN), respectively. The concentrations of antinuclear (ANA), anti-double-stranded DNA (anti-dsDNA) and anti-Sm in peripheral blood were determined using ELISA kits (Cusabio Biotech, Wuhan, Hubei, China). The absorbance value at 450 nm was measured using a multimode microplate reader (Synergy 2, BioTek).

Biochemical analysis

The 24-h urinary protein concentration, blood urea nitrogen (BUN) level, and serum creatinine (Cr) level were measured using a functional kit (Nanjing Jiancheng Bioengineering Institute, Nanjing, Jiangsu, China) according to the manufacturer's instructions.

Hematoxylin-eosin (HE) staining

Intact renal tissue sections were dried at room temperature, fixed for 30 s, stained with hematoxylin (60 °C) for 60 s, differentiated with 1% hydrochloric ethanol, counterstained with eosin for 3 min, dehydrated and permeabilized with xylene. The balsam-sealed sections were observed under a microscope (BX63, Olympus, Tokyo, Japan) to assess pathological conditions.

Based on observations of the sections, the severity of nephritis was semi-quantitatively analyzed using the following classification criteria: '0', normal; '1', mild to moderate increase in cellularity, accompanied by mesangial proliferation; '2', moderate increase in cellularity, accompanied by mesangial proliferation and endocapillaries, increased matrix and/or karyorrhexis; '3', significant increase in cellularity, accompanied by crescent formation and/or necrosis and/or sclerosis[22].

Masson's trichrome staining

The renal samples were fixed with 4% paraformaldehyde, dehydrated, embedded in paraffin and sliced into 4 μm sections, which were baked at 80 °C, dewaxed with xylene, dehydrated with 100% and 50% ethanol, stained with Weiger's iron hematoxylin (Biolab, Beijing, China), differentiated with 1% hydrochloric ethanol and stained with Ponceau S. After treatment with 1% phosphomolybdic acid, the sections were counterstained with aniline blue or green, treated with 1% acetic acid, dehydrated with 95% and 100% ethanol, permeabilized with xylene and sealed with neutral resin. An optical microscope (Olympus) was used for observation and photography.

Transmission electron microscopy (TEM)

The mouse renocortical tissues were cut into blocks (1 mm³), fixed with 2.5% glutaraldehyde and 1% acid fixative and dehydrated. The tissues were immersed in pure acetone, embedded in Epon-812 epoxy resin, baked at 35 °C, 45 °C and 65 °C and sliced into thin sections. After staining with toluidine blue, ultrathin sections were obtained under an optical microscope. Images were observed using TEM (JEOL-1230, JEOL, Akishima, Tokyo, Japan).

TUNEL staining

Dewaxed sections were incubated with proteinase K working solution and permeabilization washing buffer (Servicebio, Wuhan, Hubei, China). TdT and dUTP reagents (Roche, Basel, Switzerland) were mixed at a ratio of 2:29. The sections were combined with the mixture, incubated for 2 h, stained with DAPI (Servicebio), sealed with glycerol and observed under a fluorescence microscope (Nikon, Tokyo, Japan).

Immunofluorescence staining

Renal tissues were stained with Alexa Fluor 488-conjugated goat anti-mouse IgG H&L (A32723, 1:200, Invitrogen) and Alexa Fluor 488-conjugated IgM (A-21042, 1:200, Invitrogen). The fluorescence intensity of 10–15 randomly selected glomeruli was measured to evaluate the deposition of IgG and IgM in glomeruli and blindly scored from 0–3 (0: none; 1: weak; 2: mild; 3: strong). All images were captured using a Leica DM6B microscope equipped with a color camera.

Fra2 expression in renal tissues was measured as described below. Frozen renal tissue sections (8 μm) were fixed with 4% formaldehyde, permeabilized with 0.1% Triton X-100, blocked with 5% bovine serum albumin, incubated with primary antibody against c-Fos (sc-271243, Santa Cruz) at 4 °C overnight, incubated with different secondary antibodies, and mounted using DAPI-supplemented Vectashield fixative medium (Vector Laboratories, Burlingame, CA). Fluorescence images were visualized using a confocal laser scanning microscope (LSM700, Zeiss, Germany).

Immunochemistry

Renal tissue sections were treated with 3% H_2O_2 at room temperature for 25 min to block endogenous peroxidase, followed by the addition of citric acid buffer for antigen retrieval. Sections were blocked with normal goat serum (Sango, Shanghai, China) at room temperature for 20 min and incubated with primary antibodies against YY1 (1:250), IFN-γ (1:200), PARP-1 (1:1000) and FOXO1 (1:100) at 4 °C overnight and with goat anti-rabbit IgG (ab6721, 1:5000, Abcam) secondary antibody for 30 min. After exposure to SABC
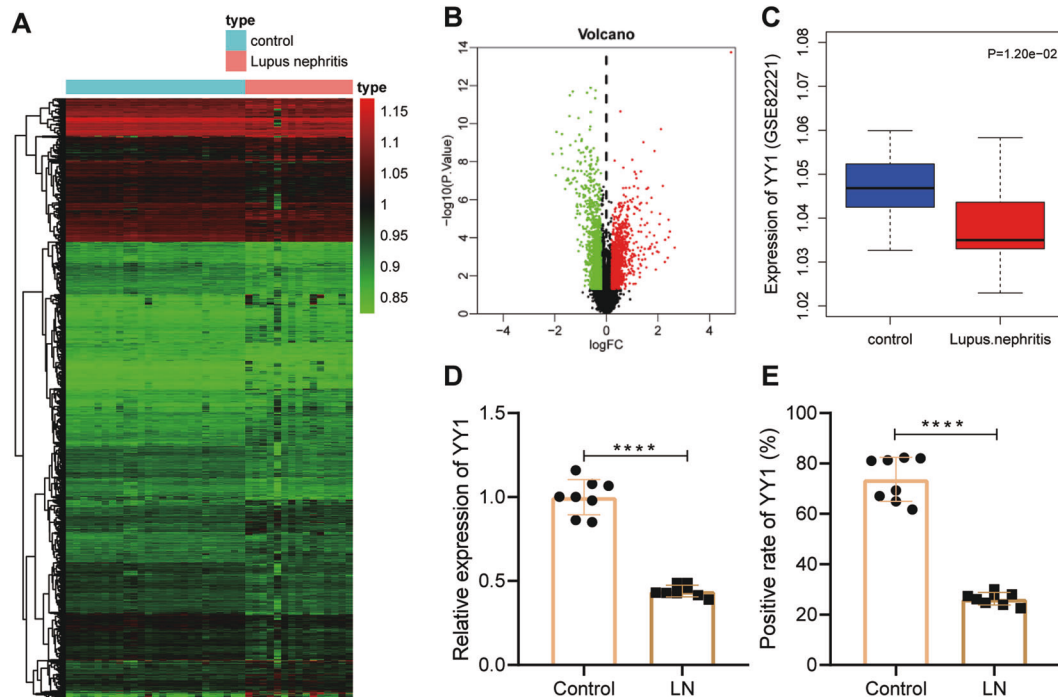
Fig. 1 YY1 expression is downregulated in renal tissues of the mice with LN. A A heatmap displaying differentially expressed mRNAs in LN samples from GSE82221. The abscissa indicates the sample number, and the ordinate indicates differentially expressed mRNAs. The histogram on the right indicates the color scale, with each rectangle referring to the expression level in each sample. **B** Volcano plot displaying differentially expressed mRNAs in LN samples from GSE82221. Red dots represent genes with upregulated expression, and green dots represent genes with downregulated expression in the LN samples. **C** YY1 expression in the LN and control samples from GSE82221. **D** YY1 expression in renal tissues of the mice with LN was determined by qRT-PCR and normalized to that of β-actin. **E** YY1 expression in renal tissues of the mice with LN identified by immunohistochemistry. ****$p < 0.0001$. Data comparisons between two groups were performed by independent sample t tests. Cell experiments were independently repeated 3 times.

(Vector Laboratories), the sections were incubated at 37 °C for 30 min, followed by development using 3,3'-diaminobenzidine (P0203, Beyotime Biotechnology, Shanghai, China). After hematoxylin staining, the sections were observed under a microscope (BX63, Olympus).

Statistical analysis
All data were processed using SPSS 21.0 software (IBM, Armonk, NY). Measurement data are expressed as the mean ± standard deviation. Data from two groups were compared using independent sample t tests, and data from multiple groups were compared using one-way analysis of variance (ANOVA) followed by Tukey's post-hoc test. Pearson's correlation analysis was performed to determine correlations. A value of $p < 0.05$ indicated statistical significance.

RESULTS
YY1 was expressed at low levels in renal tissues from mice with LN
In the current investigation, we investigated whether YY1 ameliorated LN-induced renal injury. First, YY1 expression in renal tissues from patients with LN was determined. The LN-related microarray dataset GSE82221 from the GEO database revealed 1222 genes with upregulated expression and 1387 genes with downregulated expression in samples from the patients with LN (Fig. 1A, B) following the differential expression analysis using the "limma" package of R language based on |logFoldChange| > 0.2 and $p < 0.05$. Therefore, YY1 expression was significantly downregulated in samples from the patients with LN in the GSE82221 dataset (Fig. 1C).

Subsequently, a mouse model of LN was developed, and YY1 expression was determined in the renal tissues of these mice using qRT-PCR. The results showed low YY1 expression in the renal tissues of the mice with LN (Fig. 1D). The results of immunohistochemical

staining were consistent with those of qRT-PCR (Fig. 1E). These findings indicated that YY1 expression was downregulated in renal tissues from the mice with LN.

YY1 overexpression alleviated LN-induced renal injury
After determining the YY1 expression pattern in renal tissues, we investigated the role of YY1 in LN. Biochemical tests (Fig. 2A) and ELISAs (Fig. 2B, C) revealed elevated urinary protein, serum Cr and BUN levels in the mice with LN, accompanied by high levels of ANA, anti-ds-DNA, anti-Sm, TNF-α, IL-1β and IL-6, and these levels were decreased by oe-YY1 treatment. Based on these results, YY1 improved renal function and reduced inflammation in the mice with LN.

Subsequently, pathological changes in renal tissues modulated by YY1 were shown by HE staining (Fig. 2D) and Masson's trichrome staining (Fig. 2E). Renal tissues exhibited a thicker tubular basement membrane, dilatation of renal tubules, vacuolar degeneration, glomerular swelling, and increased collagen deposition, suggesting a pathological injury similar to that observed in the patients with LN, all of which were alleviated by oe-YY1. According to TEM (Fig. 2F), little mesangial matrix was detected in the normal mice, while mesangial cells, increased proliferation of mesangial matrix and increased fibrous structure of glomerular membrane were observed in renal tissues from the mice with LN, and these changes were subsequently decreased by oe-YY1, indicating that YY1 alleviated pathological injury in renal tissues of the mice with LN.

Then, the resulting deposition of immune complexes and renal injury were detected by performing immunofluorescence staining using IgG and IgM (Fig. 2G). Stronger fluorescence signals were detected in the glomeruli of the mice with LN, suggesting greater deposition of IgG and IgM; however,
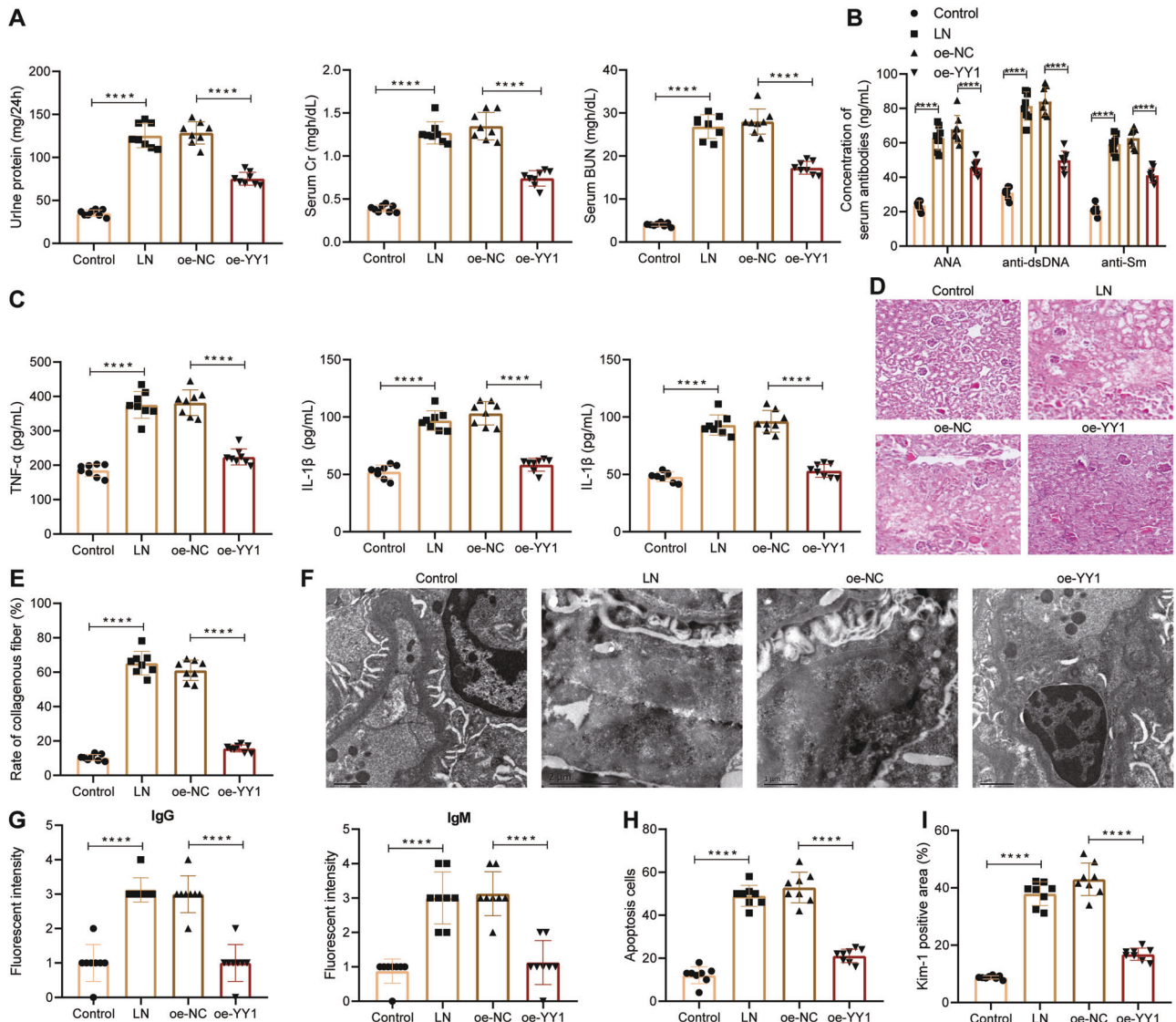
Fig. 2 YY1 exerts a renoprotective effect on the mice with LN. A Urinary protein, serum Cr and BUN levels measured by biochemical tests. **B** Concentrations of serum antibodies against ANA, dsDNA and Sm measured by ELISAs. **C** Serum contents of TNF-α, IL-1β and IL-6 measured by ELISAs. **D** Pathological changes in mouse renal tissues identified by HE staining. **E** Deposition of collagen fibers in renal tissues identified by Masson staining. **F** Mesangial cells and mesangial matrix structure in renal tissues observed under TEM. **G** Immunoglobulin deposits in renal tissues identified by immunofluorescence staining. **H** Cell apoptosis in renal tissues identified by TUNEL staining. **I** Kim-1 expression in renal tissues identified by immunofluorescence staining. $n = 8$. ****$p < 0.0001$. $n = 8$. Data comparison was performed by one-way ANOVA among multiple groups, followed by Tukey's post-hoc test. Cell experiments were independently repeated 3 times.

treatment with oe-YY1 reversed these changes. In addition, TUNEL and immunofluorescence staining revealed the induction of cell apoptosis and upregulated expression of the renal injury biomarker Kim-1, both of which were reduced by treatment with oe-YY1 (Fig. 2H, I). Thus, renal injury induced by LN was significantly alleviated by YY1.

YY1 inhibited Jurkat cell apoptosis and inflammatory factor release by suppressing IFN-γ transcription
To further investigate the regulatory mechanism underlying YY1 in LN, we predicted YY1 downstream genes utilizing the TRRUST database. YY1 was identified as an inhibitor of IFN-γ transcription, and the YY1 binding site in the IFN-γ promoter was predicted using JASPAR (Supplementary Table 3). IFN-γ was shown to be expressed at high levels in patients with LN, and IFN-γ over-expression is required to maintain the pathology of LN[9,23].

Therefore, we explored the expression pattern of IFN-γ and its role in the regulatory effects of YY1 in LN.

Upregulated mRNA and protein expression levels of IFN-γ in renal tissues of the mice with LN were confirmed using qRT-PCR (Fig. 3A), immunohistochemical staining (Fig. 3B) and Western blot analysis (Fig. 3C). Then, Jurkat cells were used to examine the efficiency of YY1 overexpression and silencing, where YY1 expression was increased by oe-YY1 but decreased by sh-YY1#1 and sh-YY1#2 (Fig. 3D). Notably, sh-YY1#2 was selected for subsequent experiments due to its higher silencing efficiency.

Then, the mechanism by which YY1 regulates IFN-γ expression was investigated. qRT-PCR results showed that IFN-γ expression was increased by sh-YY1 and reduced by oe-YY1 (Fig. 3E), indicating that YY1 downregulated IFN-γ expression. Additionally, a dual-luciferase reporter gene assay revealed that luciferase
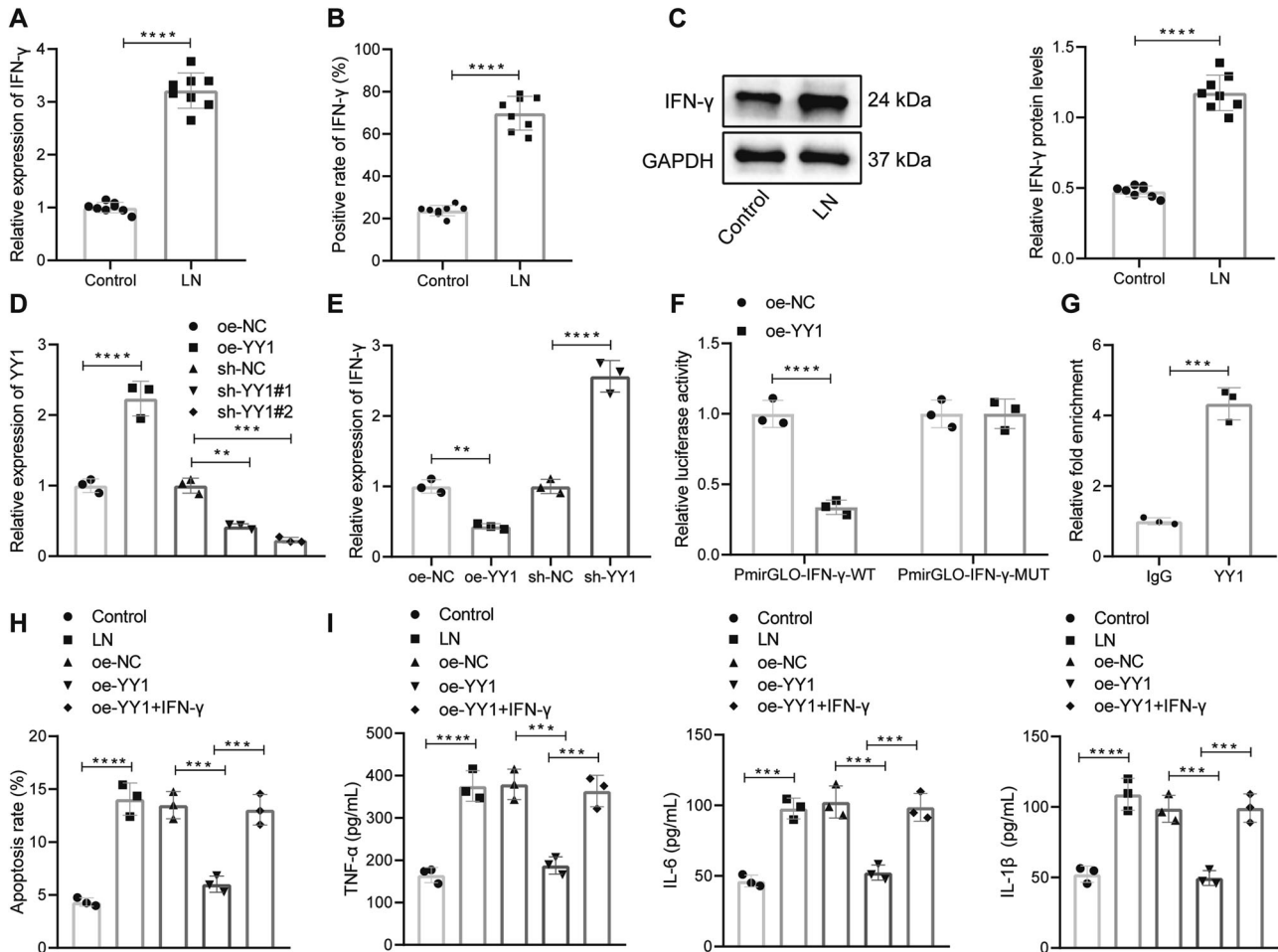
Fig. 3 The inhibitory effect of YY1 on cell apoptosis and the release of inflammatory factors depends on the modulation of IFN-γ transcription. A IFN-γ expression in renal tissues was determined by qRT-PCR and normalized to that of β-actin. **B** IFN-γ expression in renal tissues determined by immunohistochemical staining. **C** IFN-γ protein levels in renal tissues were determined by Western blot analysis and normalized to GAPDH. **D** YY1 expression in Jurkat cells was determined by qRT-PCR and normalized to that of β-actin. **E** IFN-γ expression in Jurkat cells was determined by qRT-PCR and normalized to that of β-actin. **F** Binding between YY1 and the IFN-γ promoter detected by a dual-luciferase reporter gene assay. **G** Enrichment of YY1 in the IFN-γ promoter detected by ChIP assays. **H** Jurkat cell apoptosis detected by flow cytometry. **I** Serum contents of TNF-α, IL-1β and IL-6 in cell supernatants measured by ELISAs. ****$p < 0.0001$, ***$p < 0.001$, **$p < 0.01$. $n = 8$. Data analysis was performed by independent sample t tests between two groups and by one-way ANOVA among multiple groups, followed by Tukey's post-hoc test. Cell experiments were independently repeated 3 times.

activity was weakened in response to cotransfection of PmirGLO-IFN-γ-WT with oe-YY1 relative to cotransfection with oe-NC. However, no significant difference in luciferase activity was observed in the cells cotransfected with PmirGLO-IFN-γ-MUT and oe-YY1 compared to those with oe-NC (Fig. 3F), suggesting that overexpressed YY1 inhibited IFN-γ promoter activity in Jurkat cells. Further ChIP assays demonstrated direct binding between YY1 and the IFN-γ promoter (Fig. 3G). In summary, these findings revealed that YY1 inhibited IFN-γ transcription by directly binding to the IFN-γ promoter.

Jurkat cell apoptosis and inflammatory factor release were detected to further verify the role of IFN-γ in the mechanism by which YY1 alleviates LN-induced renal injury. As shown in Fig. 3H, I, the cell apoptosis rate was higher in LN cells, accompanied by higher TNF-α, IL-1β and IL-6 levels, all of which were reversed by oe-YY1 treatment; however, further delivery of IFN-γ abrogated the effect of oe-YY1. Therefore, YY1 exerted an inhibitory effect on Jurkat cell apoptosis and inflammatory factor release that was neutralized by IFN-γ restoration.

In summary, YY1 inhibited IFN-γ transcription to suppress cell apoptosis and the release of inflammatory factors.

Downregulated IFN-γ expression inhibited Fra2 expression to suppress cell apoptosis and the release of inflammatory factors

Fra2 overexpression has been reported in patients with LN, and IFN-γ significantly increases Fra2 protein levels[10]. To further elucidate the role of IFN-γ/Fra2 in the effect of YY1 in LN, we determined Fra2 expression by performing immunofluorescence staining (Fig. 4A) and Western blot analysis (Fig. 4B). A stronger fluorescence signal and higher Fra2 protein levels were detected in renal tissues of the mice with LN.

Subsequent qRT-PCR was used to determine the efficiency of IFN-γ silencing in Jurkat cells and showed that IFN-γ expression was significantly decreased in the Jurkat cells treated with sh-IFN-γ#1 or sh-IFN-γ#2, and sh-IFN-γ#2 was selected for subsequent experiments due to the higher silencing efficiency (Fig. 4C). Western blot analysis showed that Fra2 protein levels were reduced by sh-IFN-γ (Fig. 4D). Moreover, the downregulation of YY1 expression and upregulation of IFN-γ and Fra2 expression in LN cells were reversed by oe-YY1, but this effect was counteracted by IFN-γ addition. The abovementioned results indicated that YY1 downregulated Fra2 expression by inhibiting IFN-γ.
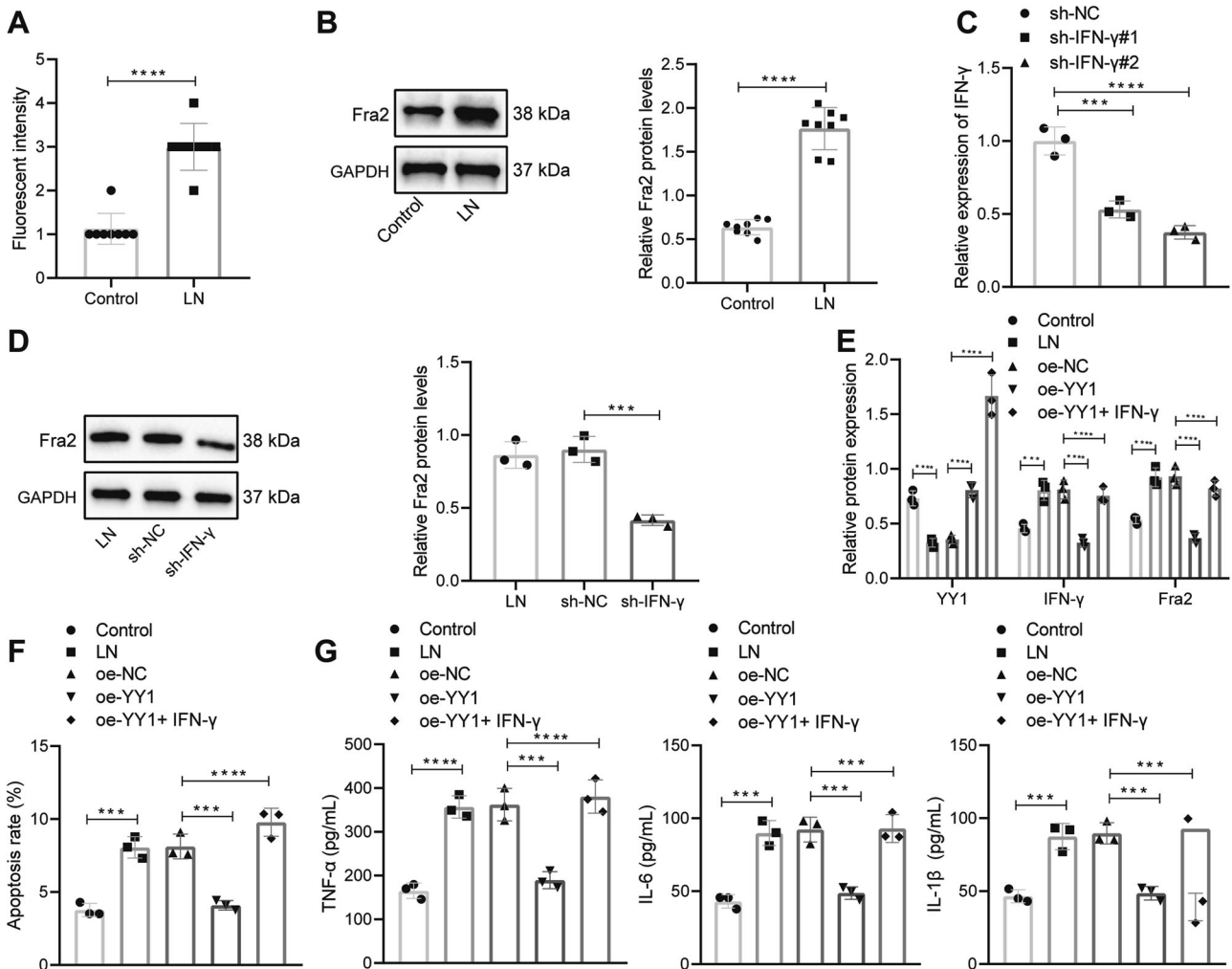
Fig. 4 IFN-γ downregulates Fra2 expression to suppress apoptosis and the release of inflammatory factors. A Fra2 expression in renal tissues identified by immunofluorescence staining. **B** Fra2 protein levels in renal tissues were determined by Western blot analysis and normalized to those of GAPDH. **C** IFN-γ expression in Jurkat cells was determined by qRT-PCR and normalized to β-actin expression. **D** Fra2 protein levels in Jurkat cells were determined by Western blot analysis and normalized to those of GAPDH. **E** Protein levels of YY1, IFN-γ and Fra2 in Jurkat cells determined by Western blot analysis normalized to those of GAPDH. **F** Jurkat cell apoptosis detected by flow cytometry. **G** Serum contents of TNF-α, IL-1β and IL-6 in cell supernatants measured by ELISAs. ****$p < 0.0001$, ***$p < 0.001$, **$p < 0.01$. $n = 8$. Data analysis was performed by independent sample t tests between two groups and by one-way ANOVA among multiple groups, followed by Tukey's post-hoc test. Cell experiments were independently repeated 3 times.

Then, we explored whether Fra2 inhibition played an important role in the effect of YY1 on LN-induced renal injury by detecting cell apoptosis and the release of inflammatory factors from Jurkat cells. Flow cytometry and ELISAs showed that YY1 overexpression led to decreased cell apoptosis and inflammatory factor levels, which were restored by Fra2 (Fig. 4F, G). These findings revealed the role of downregulation of Fra2 expression in the inhibitory effects of YY1 on Jurkat cell apoptosis and the release of inflammatory factors.

In conclusion, apoptosis of Jurkat cells and release of inflammatory factors were inhibited by YY1 through the downregulation of Fra2 expression via IFN-γ.

Downregulated Fra2 expression inhibited PARP-1 expression to suppress cell apoptosis and the release of inflammatory factors

PARP-1 has been reported to be activated in individuals with glomerulonephritis, while pharmacological inhibition of PARP-1 alleviates nephritis and improves the survival rate; moreover, downregulated Fra2 expression may inhibit PARP-1 expression[11,24].

Here, the focus of the study shifted to whether YY1 alleviated LN-induced renal injury by downregulating PARP-1 expression through Fra2 inhibition. PARP-1 expression in renal tissues of the mice with LN was first determined using Western blot analysis, and the results confirmed the upregulated PARP-1 expression in the mice with LN (Fig. 5A).

Subsequent qRT-PCR measurement of the silencing efficiency showed that Fra2 expression was substantially decreased in the Jurkat cells treated with sh-Fra2#1 or sh-Fra2#2; sh-Fra2#2 was selected for subsequent experiments due to its higher silencing efficiency (Fig. 5B). Western blot analysis showed that the PARP-1 protein level was reduced by sh-Fra2 (Fig. 5C), suggesting that Fra2 inhibition decreased PARP-1 expression. Moreover, the downregulation of YY1 expression and upregulation of PARP-1 and Fra2 expression in the LN models were reversed by oe-YY1, the action of which was counteracted by Fra2 addition (Fig. 5D). Based on these results, YY1 downregulated PARP-1 expression by inhibiting Fra2.

Furthermore, flow cytometry and ELISAs showed that YY1 overexpression decreased cell apoptosis and inflammatory factor
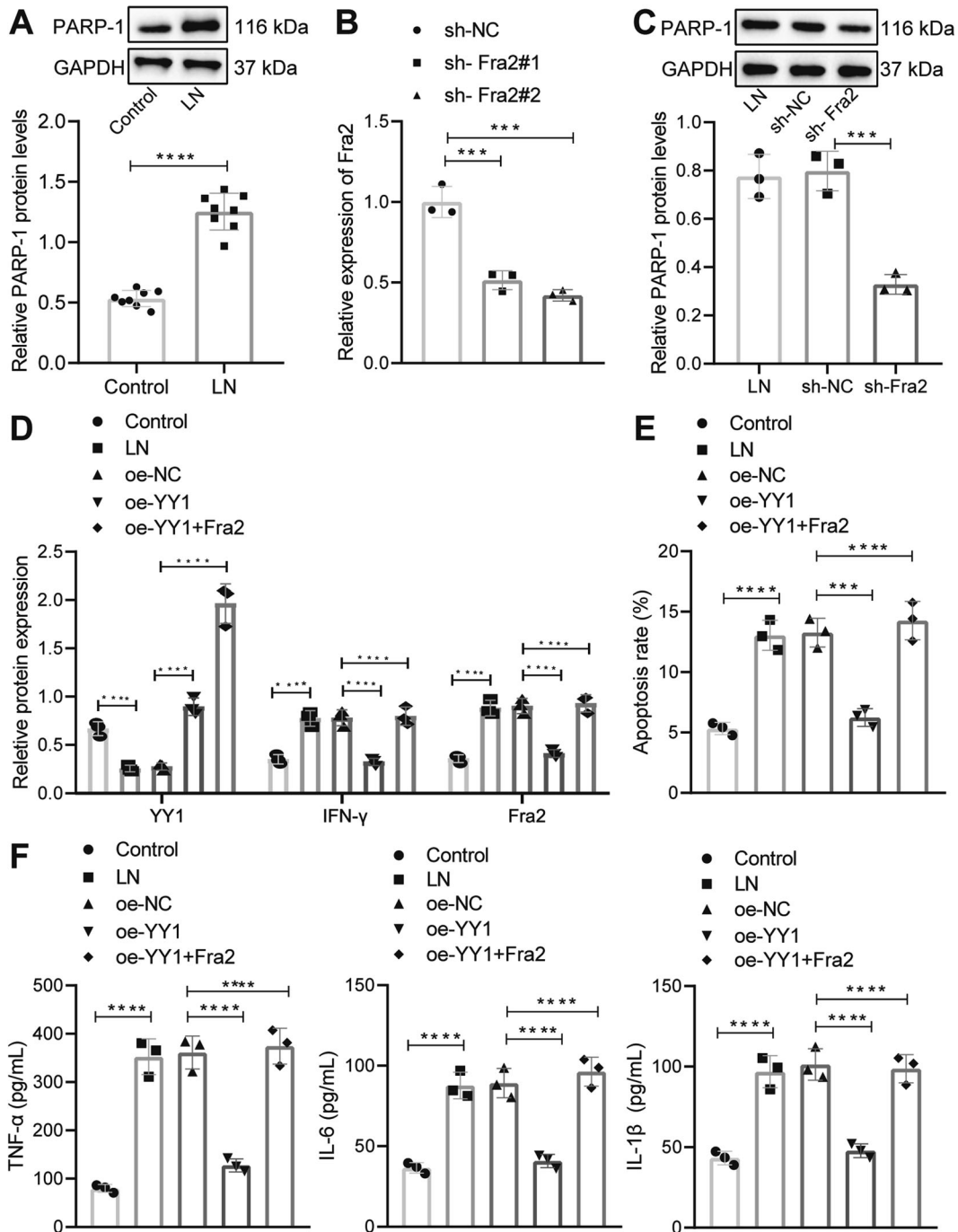
Fig. 5 Fra2 downregulates PARP-1 expression to suppress cell apoptosis and the release of inflammatory factors. A PARP-1 protein levels in renal tissues were determined by Western blot analysis and normalized to those of GAPDH. **B** Fra2 expression in Jurkat cells was determined by qRT-PCR and normalized to β-actin expression. **C** PARP-1 protein levels in Jurkat cells were determined by Western blot analysis and normalized to GAPDH levels. **D** Protein levels of YY1, Fra2 and PARP-1 in Jurkat cells determined by Western blot analysis and normalized to GAPDH levels. **E** Jurkat cell apoptosis detected by flow cytometry. **F** Serum contents of TNF-α, IL-1β and IL-6 in cell supernatants measured by ELISAs. ****$p < 0.0001$, ***$p < 0.001$, **$p < 0.01$. $n = 8$. Data analysis was performed by independent sample t tests between two groups and by one-way ANOVA among multiple groups, followed by Tukey's post-hoc test. Cell experiments were independently repeated 3 times.

levels, which were restored by PARP-1 overexpression (Fig. 5E, F). These findings revealed the role of downregulated PARP-1 expression in the inhibitory effect of YY1 on Jurkat cell apoptosis and the release of inflammatory factors.

In conclusion, apoptosis of Jurkat cells and release of inflammatory factors were suppressed by YY1 through Fra2 inhibition and subsequent downregulation of PARP-1 expression.

Downregulation of PARP-1 expression promoted FOXO1 expression to suppress cell apoptosis and the release of inflammatory factors

FOXO1 has been proposed to function as a protective factor in renal disorders, and PARP-1 may be negatively correlated with FOXO1 expression[12,25]. Hence, we aimed to explore whether YY1 mediated FOXO1 expression by regulating PARP-1. FOXO1
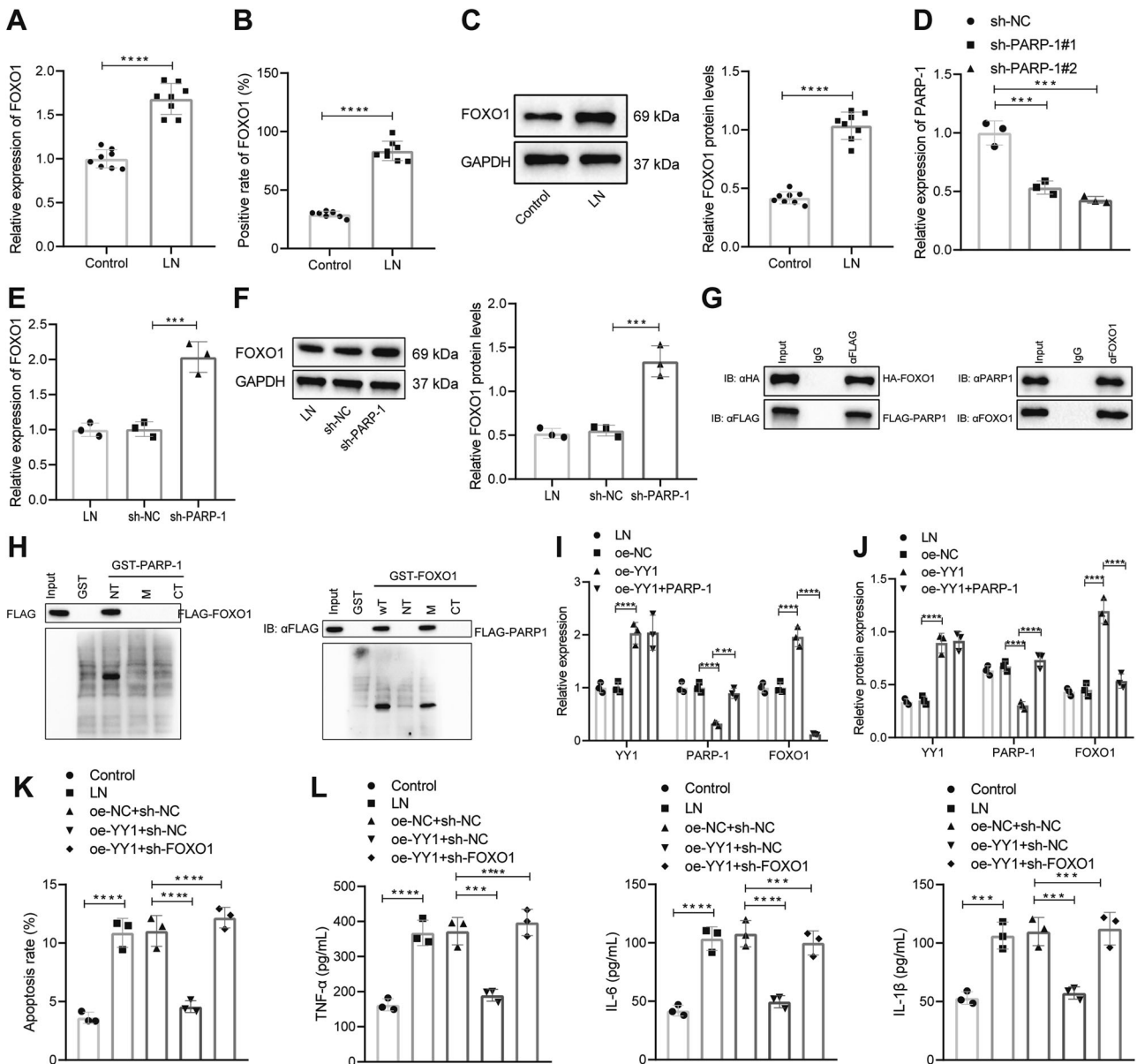
B. Wang et al.

Fig. 6 PARP-1 silencing upregulates FOXO1 expression to suppress cell apoptosis and the release of inflammatory factors. A FOXO1 expression in renal tissues was determined by qRT-PCR and normalized to β-actin expression. **B** FOXO1 expression in renal tissues identified by immunofluorescence staining. **C** PARP-1 protein levels in renal tissues were determined by Western blot analysis and normalized to GAPDH levels. **D** PARP-1 expression in Jurkat cells was determined by qRT-PCR and normalized to β-actin expression. **E** FOXO1 expression in Jurkat cells was determined by qRT-PCR and normalized to β-actin expression. **F** FOXO1 protein level in Jurkat cells determined by Western blot analysis and normalized to that of GAPDH. **G** Interaction between PARP-1 and FOXO1 in Jurkat cells detected by Co-IP assays. **H** Interaction between PARP-1 and FOXO1 in vitro detected by GST pulldown assays. **I** Expression of YY1, PARP-1 and FOXO1 in Jurkat cells was determined by qRT-PCR and normalized to β-actin expression. **J** Protein levels of YY1, PARP-1 and FOXO1 in Jurkat cells determined by Western blot analysis and normalized to GAPDH levels. **K** Jurkat cell apoptosis detected by flow cytometry. **L** Serum contents of TNF-α, IL-1β and IL-6 in cell supernatants measured by ELISAs. ****$p < 0.0001$, ***$p < 0.001$. $n = 8$. Data analysis was performed by independent sample t tests between two groups and by one-way ANOVA among multiple groups, followed by Tukey's post-hoc test. Cell experiments were independently repeated 3 times.

expression in renal tissues of the mice with LN was first determined using qRT-PCR, immunohistochemical staining and Western blot analysis, and the results revealed reduced FOXO1 levels (Fig. 6A–C).

Subsequently, qRT-PCR was performed to determine the efficiency of PARP-1 silencing in Jurkat cells, and PARP-1 expression was significantly decreased in the Jurkat cells treated with sh-PARP-1#1 or sh-PARP-1#2. Notably, sh-PARP-1#2 was selected for subsequent experiments due to its higher silencing efficiency (Fig. 6D). Furthermore, qRT-PCR and Western blot

analysis showed that FOXO1 protein levels were increased by sh-PARP-1 (Fig. 6E, F), suggesting that PARP-1 inhibition promoted FOXO1 expression.

For further analyses, Jurkat cells were transiently transfected with FLAG-PARP-1 and HA-FOXO1, followed by Co-IP using anti-FLAG antibody and an immunoblotting assay using anti-HA antibody. The results showed that PARP-1 could interact with FOXO1 in vivo, confirming the binding between endogenous FOXO1 and PARP-1 in Jurkat cells (Fig. 6G). Subsequent GST pulldown assays revealed in vitro binding between FOXO1 and the PARP-1 N-terminus, which
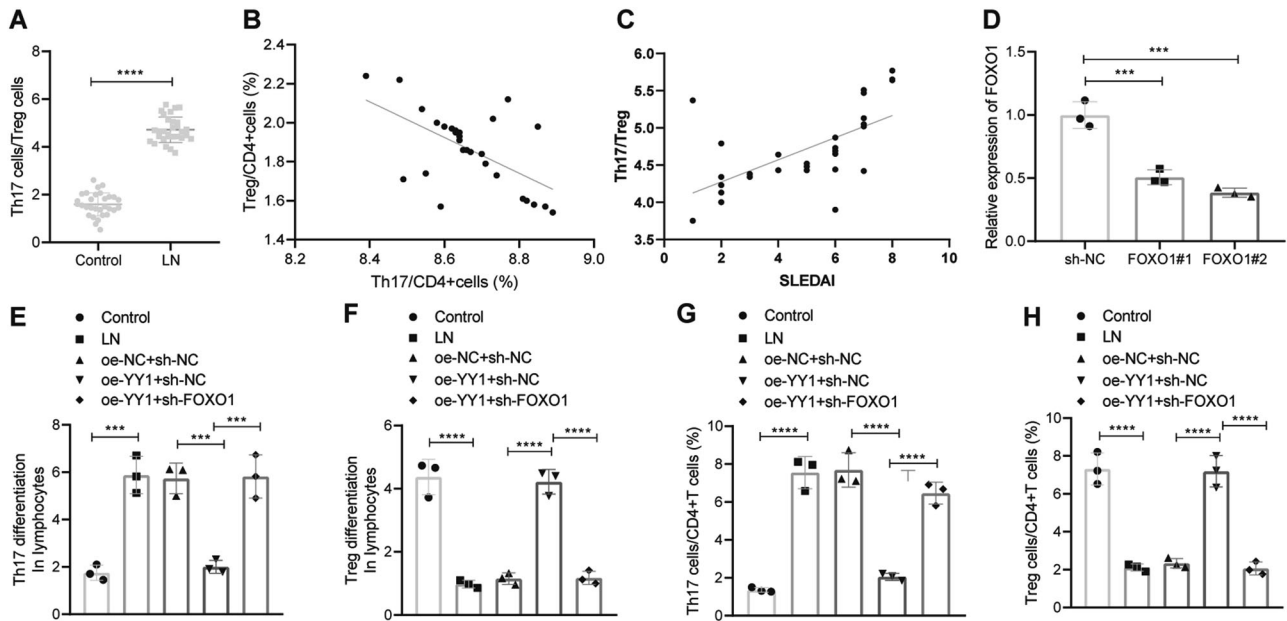
Fig. 7 YY1 reduces the Th17/Treg cell ratio by upregulating FOXO1 expression. A Th17/Treg cell ratio in the peripheral blood of patients with LN and healthy subjects. **B** Correlation analysis between Th17 cells and Treg cells in the peripheral blood of patients with LN. **C** Correlation analysis between the Th17/Treg cell ratio and SLEDAI. **D** FOXO1 expression in cells was determined by qRT-PCR and normalized to β-actin expression. **E** Th17 differentiation in lymphocytes detected by flow cytometry. **F** Treg cell differentiation in lymphocytes detected by flow cytometry. **G** Th17 cells in the peripheral blood of mice with LN detected by flow cytometry. **H** Treg cells in the peripheral blood of mice with LN detected by flow cytometry. ****$p < 0.0001$, ***$p < 0.001$. $n = 8$. Data analysis was performed by independent sample t tests between two groups and by one-way ANOVA among multiple groups, followed by Tukey's post-hoc test. Pearson's correlation analysis was introduced for correlation analysis. Cell experiments were independently repeated 3 times.

interacted with the middle region of FOXO1 (Fig. 6H). Thus, PARP-1 directly interacted with FOXO1. Because PARP-1 inhibition directly promoted FOXO1 expression, we investigated whether YY1 mediated FOXO1 expression via PARP-1. As shown in Fig. 6I, J, qRT-PCR and Western blot analysis revealed the YY1-mediated promotion of FOXO1 expression, while PARP-1 blocked this effect to decrease FOXO1 expression. Based on these findings, YY1 promoted FOXO1 expression by inhibiting PARP-1.

Flow cytometry and ELISAs showed that overexpressed YY1 decreased cell apoptosis and inflammatory factor levels, which were restored by silencing FOXO1 (Fig. 6K, L). These findings indicated that the inhibitory effect of YY1 on Jurkat cell apoptosis and the release of inflammatory factors depended on upregulation of FOXO1 expression.

Thus, the apoptosis of Jurkat cells and the release of inflammatory factors were suppressed by YY1 through PARP-1 inhibition and the subsequent upregulation of FOXO1 expression.

FOXO1 decreased the Th17/Treg cell ratio to alleviate LN
As shown in a previous study, FOXO1 may inhibit Th17 cell differentiation and promote the production of Treg cells[26]. In addition, LN is alleviated through a reduction in the Th17/Treg cell ratio[27]. The Th17/Treg cell ratio in the peripheral blood of the patients with LN and the healthy subjects was determined, and the results revealed a significantly higher Th17/Treg cell ratio in the patients with LN than in the healthy subjects (Fig. 7A). Subsequent flow cytometric analysis revealed an inverse relationship between Th17 cells and Treg cells in the peripheral blood of the patients with LN (Fig. 7B). The association of the Th17/Treg cell ratio with LN was then investigated. The Th17/Treg cell ratio in peripheral blood was increased with an increase in the SLE disease activity (SLEDAI score) (Fig. 7C).

We then investigated whether YY1 decreased the Th17/Treg cell ratio by upregulating FOXO1 expression. Based on the qRT-PCR detection of the efficiency of FOXO1 silencing in Jurkat cells, sh-

FOXO1#2 was selected for subsequent experiments due to its higher silencing efficiency (Fig. 7D). Next, the flow cytometric analysis revealed more Th17 cells and fewer Treg cells in LN; these increases were reversed by YY1 overexpression, and additional silencing of FOXO1 counteracted the effect of overexpressed YY1 (Fig. 7E, F). Consistent results were observed in mouse peripheral blood (Fig. 7G, H). These findings indicated that YY1 reduced the Th17/Treg cell ratio by increasing FOXO1 expression.

To further verify the involvement of the Th17/Treg cell ratio in the ability of YY1 to alleviate LN, we treated mice with different protocols. Biochemical tests (Fig. 8A) and ELISAs (Fig. 8B, C) revealed reduced urinary protein, serum Cr and BUN levels in the mice with LN overexpressing YY1, accompanied by lower levels of ANA, anti-ds-DNA, anti-Sm, TNF-α, IL-1β and IL-6, and all of these effects were reversed by further sh-FOXO1 treatment. Subsequently, pathological changes in renal tissues were observed using HE staining and graded accordingly (Fig. 8D, E), and cell apoptosis was detected by TUNEL staining (Fig. 8F) following euthanasia. Renal tissues exhibited a thicker tubular basement membrane and more mesangial cells in the presence of over-expressed YY1 accompanied by reduced cell apoptosis, and these effects were further increased by sh-FOXO1.

These lines of evidence suggested that YY1 alleviates LN by reducing the Th17/Treg cell ratio through the upregulation of FOXO1 expression.

DISCUSSION
In the present study, we investigated the effects and underlying mechanism of YY1 in renal injury induced by LN. Notably, the experimental data collectively indicated that YY1 mitigated LN-induced renal injury by reducing the Th17/Treg cell ratio via the IFN-γ/Fra2/PARP-1/FOXO1 axis (Fig. 9).

Initially, decreased YY1 expression was detected in the subjects with LN, and the restoration of YY1 expression in the renal tissues
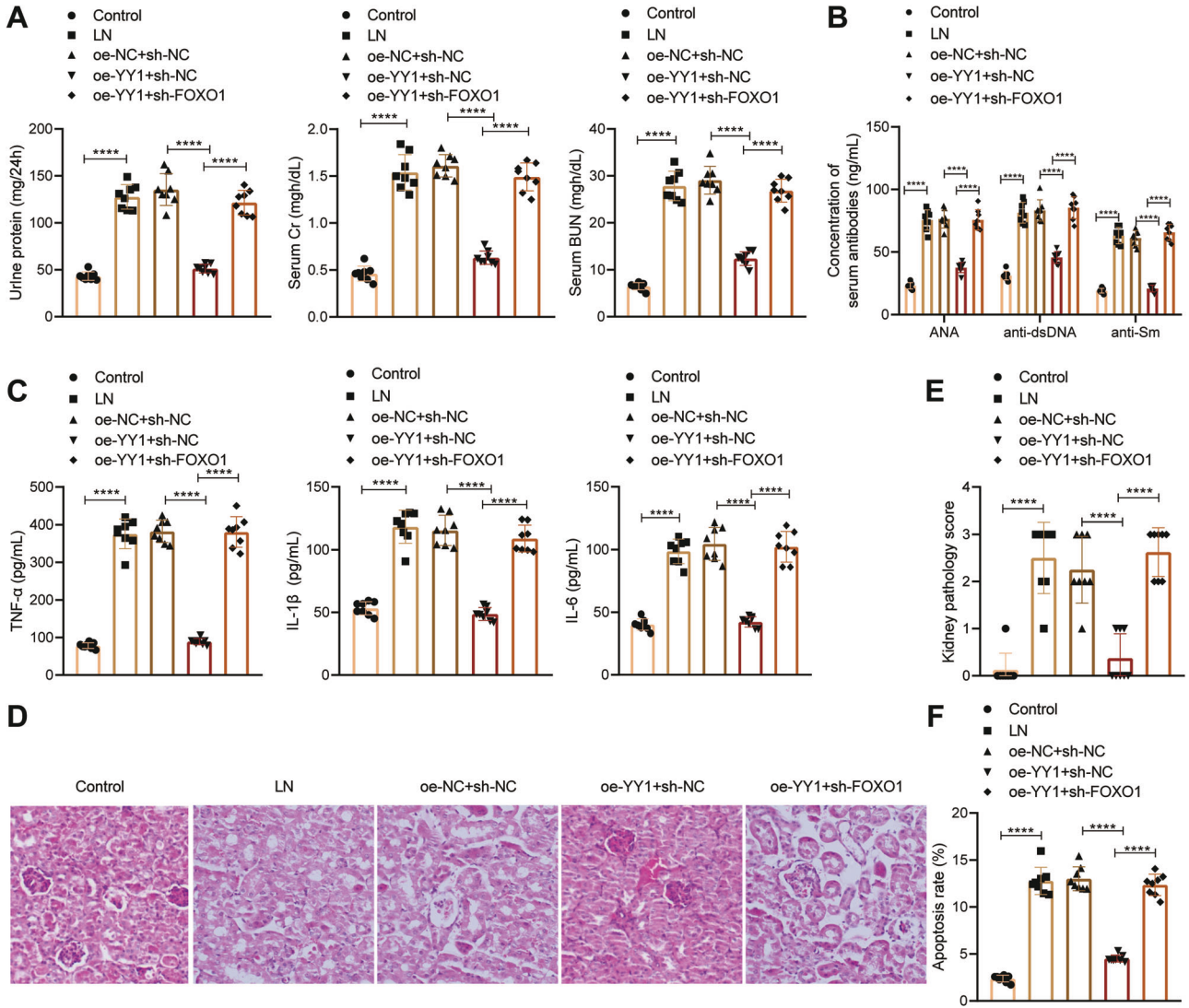
Fig. 8 YY1 decreases the Th17/Treg cell ratio to alleviate LN. A Urinary protein, serum Cr and BUN contents measured by biochemical tests. **B** Concentrations of serum antibodies against ANA, dsDNA and Sm measured by ELISAs. **C** Serum contents of TNF-α, IL-1β and IL-6 measured by ELISAs. **D** Pathological changes in mouse renal tissues identified by HE staining. **E** Kidney pathology scoring based on HE staining. **F** Cell apoptosis in renal tissues identified by TUNEL staining. $n = 8$. ****$p < 0.0001$. ***$p < 0.001$. $n = 8$. Data analysis was performed by one-way ANOVA among multiple groups, followed by Tukey's post-hoc test. Cell experiments were independently repeated 3 times.
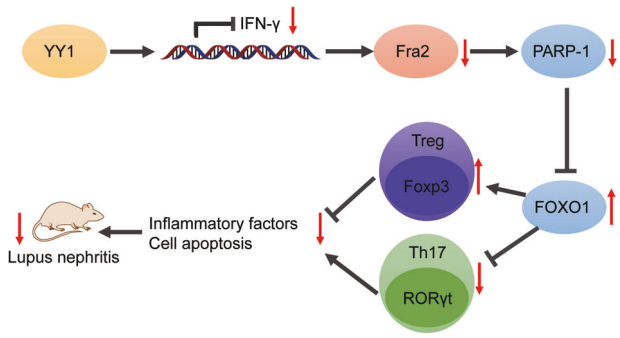

Fig. 9 Schematic diagram displaying the regulatory mechanism of YY1 in LN. YY1 alleviates LN by reducing the Th17/Treg cell ratio through PARP-1 inhibition-induced upregulation of FOXO1 expression, which is attributed to Fra2 inhibition induced by the suppression of IFN-γ promoter activity.

of the mice with LN ameliorated LN-induced renal injury. Consistent with our findings, high YY1 expression in renal tissues of patients with LN was shown to correspond to a favorable prognosis, while patients with low YY1 expression had a poor prognosis[28]. Dongre et al. suggested that YY1 functions as a modulator of transcription of the SLE-associated CS1 gene[29]. Further mechanistic investigations showed that YY1 inhibited Jurkat cell apoptosis and inflammatory factor release by suppressing IFN-γ transcription. Notably, an association between IFN-γ and lupus pathology has been identified; excess IFN-γ increases the accumulation of T follicular helper cells, indicating that IFN-γ overproduction is a necessary condition to sustain pathology related to lupus[23]. An IFN-γ response gradient in individuals with LN has been identified through integrated urinary proteomics and renal single-cell genomics[30].

Furthermore, our data indicated that restoring YY1 expression reduced Fra2 protein levels by suppressing the activity of the IFN-γ promoter, thereby downregulating PARP-1 expression. By confirming

upregulated Fra2 expression in renal tissues of the mice with LN, our study corroborates prior documentation of an increase in Fra2 protein expression in kidney biopsies from patients with LN compared with healthy controls and patients with other kidney diseases[10]. As a well-known proinflammatory cytokine responsible for the development of systemic autoimmunity, IFN-γ has been extensively implicated in the physiopathology of SLE[31,32]. Specifically, in LN, the production of IFN-γ may influence the histological phenotype of the disease[33]. Anti-IFN-γ treatment has been shown to attenuate the severity of LN[34]. Consistent with our findings, IFN-γ, which effectively increased Fra2 protein expression, was shown to induce podocyte damage, which is alleviated by the downregulation of Fra2 expression[10]. Moreover, the suppression of PARP-1 expression in LN models induced by Fra2 inhibition in our study was partially consistent with a previous investigation showing that upregulation of Fra-2 expression led to increased expression of PARP-1 in subjects with light-induced retinal damage[11]. Additionally, PARP-1 has been reported as a key mediator of necrotic cell death in the process of LN, as observed in a murine model characterized by a strong male sex specificity[24].

Moreover, we established that downregulation of PARP-1 expression could elevate FOXO1 expression and thus reduce the Th17/Treg cell ratio, alleviating LN. FOXO1 expression was upregulated in renal tissues of the mice with LN in our study, consistent with a previous study in which FOXO1 levels were reduced in blood samples from patients with LN accompanied by a high chronicity index[25]. An imbalance of Th17/Treg cells is implicated in LN development because of proinflammatory cytokine secretion that stimulates B cells to produce autoantibodies that contribute to further organ damage[35]. Furthermore, the role of the Th17/Treg cell balance in the pathogenesis of renal injury in LN has become increasingly important; increasingly more Th17 cells and fewer Treg cells are observed in patients with active proliferative LN, both of which are further reversed after 6 months of Eurolupus induction therapy[36,37], validating our results.

In summary, the aforementioned findings demonstrated the therapeutic potential of YY1 in renal injury following LN. Mechanistically, the current investigation showed that YY1 decreased the Th17/Treg cell ratio by upregulating FOXO1 expression through PARP-1 inhibition, which was attributed to downregulated Fra2 expression through inhibition of the activity of the IFN-γ promoter (Fig. 9). Nevertheless, further investigations on the physiological and pathophysiological differences between animal results and the human clinical setting are warranted.

DATA AVAILABILITY
The data that support the findings of this study are available in the manuscript and Supplementary Materials.

REFERENCES
1. Yung, S., Yap, D. Y. & Chan, T. M. A review of advances in the understanding of lupus nephritis pathogenesis as a basis for emerging therapies. 9, F1000Res (2020).
2. Caster, D. J. & Powell, D. W. Utilization of Biomarkers in Lupus Nephritis. Adv. Chronic. Kidney Dis. 26, 351–359 (2019).
3. Parikh, S. V., Almaani, S., Brodsky, S. & Rovin, B. H. Update on Lupus Nephritis: Core Curriculum 2020. Am. J. Kidney Dis. 76, 265–281 (2020).
4. Aziz, F. & Chaudhary, K. Lupus Nephritis: a treatment update. Curr. Clin. Pharmacol. 13, 4–13 (2018).
5. Pan, Y. Y., Yang, J. X., Xu, Y. F. & Mao, W. Yin Yang-1 suppresses CD40 ligand-CD40 signaling-mediated anti-inflammatory cytokine interleukin-10 expression in pulmonary adventitial fibroblasts by promoting histone H3 tri-methylation at lysine 27 modification on interleukin-10 promoter. Cell Biol. Int. 44, 1544–1555 (2020).
6. Meliala, I. T. S., Hosea, R., Kasim, V. & Wu, S. The biological implications of Yin Yang 1 in the hallmarks of cancer. Theranostics 10, 4183–4200 (2020).
7. Figiel, M., Lakomska, J., Dziedzicka-Wasylewska, M. & Gorecki, A. The effect of D380Y pathogenic mutation in human Yin Yang 1 on the protein's structure and function. Acta Biochim. Pol. 67, 73–77 (2020).
8. Gao, P. et al. Yin Yang 1 protein ameliorates diabetic nephropathy pathology through transcriptional repression of TGFbeta1. Sci. Transl. Med. 11, eaaw2050 (2019).
9. Wen, S. et al. IFN-gamma, CXCL16, uPAR: potential biomarkers for systemic lupus erythematosus. Clin. Exp. Rheumatol. 36, 36–43 (2018).
10. Xu, C., Miao, Y., Pi, Q., Zhu, S. & Li, F. Fra-2 is a novel candidate drug target expressed in the podocytes of lupus nephritis. Clin. Immunol. 197, 179–185 (2018).
11. Lv, J. & Xing, Y. Down-regulation of Fra-2 alleviates light-induced retina damage by inhibiting the PARP-1/AIF pathway. Int. J. Clin. Exp. Pathol. 11, 4221–4229 (2018).
12. Sakamaki, J., Daitoku, H., Yoshimochi, K., Miwa, M. & Fukamizu, A. Regulation of FOXO1-mediated transcription and cell proliferation by PARP-1. Biochem. Biophys. Res. Commun. 382, 497–502 (2009).
13. Greer, E. L. & Brunet, A. FOXO transcription factors at the interface between longevity and tumor suppression. Oncogene 24, 7410–7425 (2005).
14. Martinelli, I. et al. Galanin promotes autophagy and alleviates apoptosis in the hypertrophied heart through FoxO1 pathway. Redox Biol. 40, 101866 (2021).
15. Chen, J., Lu, Y., Tian, M. & Huang, Q. Molecular mechanisms of FOXO1 in adipocyte differentiation. J. Mol. Endocrinol. 62, R239–R253 (2019).
16. Ren, H. et al. Metformin alleviates oxidative stress and enhances autophagy in diabetic kidney disease via AMPK/SIRT1-FoxO1 pathway. Mol. Cell Endocrinol. 500, 110628 (2020).
17. Huang, F. et al. FoxO1-mediated inhibition of STAT1 alleviates tubulointerstitial fibrosis and tubule apoptosis in diabetic kidney disease. EBioMedicine 48, 491–504 (2019).
18. Ji, L. et al. FOXO1 Overexpression attenuates tubulointerstitial fibrosis and apoptosis in diabetic kidneys by Ameliorating Oxidative Injury via TXNIP-TRX. Oxid. Med. Cell Longev. 2019, 3286928 (2019).
19. Rong, Z., Wang, Z., Wang, X., Qin, C. & Geng, W. Molecular interplay between linc01134 and YY1 dictates hepatocellular carcinoma progression. J. Exp. Clin. Cancer Res. 39, 61 (2020).
20. Singh, R. et al. The non-steroidal anti-inflammatory drugs Sulindac sulfide and Diclofenac induce apoptosis and differentiation in human acute myeloid leukemia cells through an AP-1 dependent pathway. Apoptosis 16, 889–901 (2011).
21. Shao, D. et al. A functional interaction between Hippo-YAP signalling and FoxO1 mediates the oxidative stress response. Nat. Commun. 5, 3315 (2014).
22. Mannoor, K., Matejuk, A., Xu, Y., Beardall, M. & Chen, C. Expression of natural autoantibodies in MRL-lpr mice protects from lupus nephritis and improves survival. J. Immunol. 188, 3628–3638 (2012).
23. Lee, S. K. et al. Interferon-gamma excess leads to pathogenic accumulation of follicular helper T cells and germinal centers. Immunity 37, 880–892 (2012).
24. Jog, N. R., Dinnall, J. A., Gallucci, S., Madaio, M. P. & Caricchio, R. Poly(ADP-ribose) polymerase-1 regulates the progression of autoimmune nephritis in males by inducing necrotic cell death and modulating inflammation. J. Immunol. 182, 7297–7306 (2009).
25. Wang, X. et al. Inhibition of microRNA-182-5p contributes to attenuation of lupus nephritis via Foxo1 signaling. Exp. Cell Res. 373, 91–98 (2018).
26. Gibson, S. A., Yang, W., Yan, Z., Qin, H. & Benveniste, E. N. CK2 Controls Th17 and Regulatory T cell differentiation through inhibition of FoxO1. J. Immunol. 201, 383–392 (2018).
27. You, G. et al. MicroRNA-10a-3p mediates Th17/Treg cell balance and improves renal injury by inhibiting REG3A in lupus nephritis. Int. Immunopharmacol. 88, 106891 (2020).
28. Marquez-Marin, R. et al. [Ying-Yang (YY-1) expression and Fas in biopsies of children with type IV lupus nephritis correlates with the clinical condition]. Reumatol. Clin. 3, 117–125 (2007).
29. Dongre, P., Mathew, S., Akopova, I., Gryczynski, I. & Mathew, P. YY1 and a unique DNA repeat element regulates the transcription of mouse CS1 (CD319, SLAMF7) gene. Mol. Immunol. 54, 254–263 (2013).
30. Fava, A. et al. Integrated urine proteomics and renal single-cell genomics identify an IFN-gamma response gradient in lupus nephritis. JCI Insight 5, e138345 (2020).
31. Pollard, K. M., Cauvi, D. M., Toomey, C. B., Morris, K. V. & Kono, D. H. Interferon-gamma and systemic autoimmunity. Discov. Med. 16, 123–131 (2013).
32. Thomason, J. L., Obih, U. M., Koelle, D. M., Lood, C. & Hughes, A. G. An interferon-gamma release assay as a novel biomarker in systemic lupus erythematosus. Rheumatology (Oxford) 59, 3479–3487 (2020).
33. Miyake, K. et al. Genetically determined interferon-gamma production influences the histological phenotype of lupus nephritis. Rheumatology (Oxford) 41, 518–524 (2002).
34. Schmidt, T. et al. Function of the Th17/interleukin-17A immune response in murine lupus nephritis. Arthritis Rheumatol. 67, 475–487 (2015).
35. Fu, D., Senouthai, S., Wang, J. & You, Y. Vasoactive intestinal peptide ameliorates renal injury in a pristane-induced lupus mouse model by modulating Th17/Treg balance. BMC Nephrol. 20, 350 (2019).

36. Xing, Q., Wang, B., Su, H., Cui, J. & Li, J. Elevated Th17 cells are accompanied by FoxP3+ Treg cells decrease in patients with lupus nephritis. *Rheumatol. Int.* **32**, 949–958 (2012).

37. Shenoy, S. et al. Effect of induction therapy on circulating T-helper 17 and T-regulatory cells in active proliferative lupus nephritis. *Int. J. Rheum Dis.* **21**, 1040–1048 (2018).

AUTHOR CONTRIBUTIONS
X.J., X.S. and Z.H. conceived and designed the research. B.W. and X.S. performed the experiments. Y.L., H.X. and B.Y. analyzed the data. X.J., B.Y. and J.Q. interpreted the results of the experiments. B.W. prepared the figures. B.W., X.J. and J.Q. drafted the manuscript. Z.H., Y.L. and H.X. edited and revised the manuscript. All authors approved the final version of the manuscript.

FUNDING

COMPETING INTERESTS
The authors declare no competing interests.

ETHICS APPROVAL AND CONSENT TO PARTICIPATE
Informed consent was obtained from the enrolled subjects under a protocol approved by the Ethics Committee of Guiyang Maternal & Child Health Care Hospital. The experimental procedures involving animals were approved by the Animal Ethics Committee of Guiyang Maternal & Child Health Care Hospital. All animals received humane care according to the Guide for the Care and Use of Laboratory Animals published by the US National Institute of Health.

ADDITIONAL INFORMATION
Supplementary information The online version contains supplementary material available at https://doi.org/10.1038/s41374-022-00777-9.

Correspondence and requests for materials should be addressed to Zhi Huang or Xiaoshan Shao.

Reprints and permission information is available at http://www.nature.com/reprints

Publisher's note Springer Nature remains neutral with regard to jurisdictional claims in published maps and institutional affiliations.